Response of an asymmetrical five-story building in Fairbanks during the November 30, 2018 M7.1 Anchorage, Alaska earthquake

Mehmet Çelebi[a] and Natalia A. Ruppert[b]

(a) U.S. Geological Survey, Earthquake Science Center, Menlo Park, California

(celebi@usgs.gov)

(b) Alaska Earthquake Center, University of Alaska Fairbanks, Fairbanks, Alaska

(naruppert@alaska.edu)

ABSTRACT

A recently constructed, five-story, asymmetrical steel building on the campus of the University of Alaska, Fairbanks was equipped with a strong-motion array that recorded the M7.1 Anchorage earthquake of November 30, 2018, at an epicentral distance of 408 km. The largest recorded peak accelerations at the basement and top of the building are 0.021g and 0.071g, respectively. The steel building is designed with several bays that utilize K-shaped buckling restrained braces. The building response records allow identification of fundamental periods (frequencies) as 0.73s (1.4 Hz), 0.63s (1.60 Hz), and 0.56s (1.78 Hz) in the NS, EW, and torsional directions, respectively. System identification computations resulted in estimated critical damping percentages as 7.7 % and 4.7 % in the NS and EW directions, respectively. At this low-level of shaking, the building is not expected to (and did not) experience observable damage, which is confirmed with very small average drift ratios. This is the first time a seismic response from this structural array has been analyzed.

INTRODUCTION

The November 30, 2018, M7.1 Anchorage earthquake occurred in south-central Alaska under the most densely instrumented part of the Alaska regional seismic network, including the Anchorage strong motion array. The earthquake occurred at 8:29 AKST and was located at 61.346N and 149.955W at 46.7 km depth (*West et al*., 2019). The earthquake was captured by a few structural building recording arrays located in Anchorage. A cursory study of the recorded responses of three of these instrumented buildings have been previously published (*Çelebi*, 2019). The Anchorage earthquake occurred about a year after the Engineering Learning and Innovation Facility (ELIF) building, located on the campus of the University of Alaska, Fairbanks (UAF), was constructed and equipped with a strong motion monitoring array. In this paper, we present data recorded at the ELIF seismic array during the Anchorage earthquake and results of our analysis of those data (see Data and Resources). This analysis is the first time earthquake response data from this structural monitoring array has been studied.

ELIF is a five-story (+ one story basement) building located at 64.8553N, 147.8181W, 184 m elevation, and 408 km epicentral distance. The most prevalent features of ELIF are that it is (1) an asymmetrical building, (2) a steel construction, and (3) designed with multiple K-braced (or V-braced) and buckling restrained braced frames (BRBFs). Buckling restrained braces (BRBs) have hollow structural shapes (HSS) that are filled with grout around the plate brace. Floors are concrete slabs over steel decks. Pictures of the building during construction (obtained from Google Earth) are provided in Figure 1. The comparative level of accelerations recorded during the earthquake by the ELIF array and the Fairbanks strong motion network were recorded at 10 free-field and building sites, as shown in in Table 1. East-west peak accelerations recorded at the basement of the ELIF array were larger than those recorded at nearby free-field sites and by the Fairbanks network (Table 1).

Table 1. *Acceleration levels at ELIF (at epicentral distance of ~ 408 km) and nearby free-field stations in Fairbanks, recorded during the Anchorage earthquake.*

	Basement		Penthouse		Free-Field in Fairbanks	
	NS	EW	NS	EW	Nearby The Building	in Fairbanks
Peak Accel. (g)	0.021	0.015	0.059	0.071	~0.012	0.003- 0.0116

Figure 1*. Aerial photos of the building during construction (obtained from Google Earth). The picture on the right depicts the topography and treeless patches that reveal the surficial geology.*

The general geology of Fairbanks, Alaska, is described by *Pewe et al*. (1976) and *Wilson et al*. (2015) as "outcrops of pre-Jurassic metamorphic calc-mica schist" and "Permian Yukon-Tanana crystalline complex", which includes schists. Specifically, the site of the ELIF building constructed on the UAF campus sits on a hillside composed of mostly bedrock (see orange patches in Figure 1, right) or stiff soil (site class D). The latter information is included in the seismic design criteria of the building, as dictated by International Building Code (IBC) 2009 edition that includes 20% snow loads. Beyond this, we do not have detailed information on local geology or the geotechnical layer (GTL) below the foundation of the building. The seismic design criteria also reveal that the building design is based on importance factor =1.25, seismic use group = 3, seismic design category = D, the mapped "risk targeted maximum considered earthquake" (MCE_R), 5% damped spectral acceleration parameter at short periods, Ss =1.12 g, and S (or zero period acceleration [ZPA])=0.31g. Thus, it can be clearly stated that the design zero period acceleration is much greater than the largest peak acceleration (0.021 g; Table 1) recorded at the basement of the building.

SEISMIC MONITORING ARRAY

UAF's ELIF building was instrumented with an array of strong motion sensors shortly after its completion in the Fall of 2017. This effort was funded by the UAF's College of Engineering and Mines and by the Alaska Earthquake Center, which has been acquiring and archiving the seismic structural response data. The array comprises seven tri-axial ETNA2[1] accelerometers, deployed at five levels (Figure 2). The triaxial accelerometers are deployed at five south locations, including the basement, the 1st, the 3rd, and the 4th floors and the penthouse (ceiling of 5th floor) at the intersection of grid lines 1 and I, and at two north locations on 3rd floor and penthouse [ceiling of 5th floor]) at the intersection of grid lines 1 and B. There is no free-field station associated with the array. Figure 2 also shows the reference north and the orientations of channels of each of the tri-axial accelerometers. We follow the orientation convention used by the array developers; orientation 1 is NS, 2 is EW, and 3 is UP. The sensors located at grid lines 1 and B are designated to be in the north location. Similarly, sensors at grid lines 1 and I are designated to be in the south location. Typical BRBF elevations depicting K-bracing with BRBs and details at connections (and connection plates [CP]) according to the gridlines depicted in Figure 2a are provided in Figure 3.

We note that the seismic monitoring array comprises seven triaxial sensors, and therefore, a total of 21 channels. Hence, in this array, with the exception of the vertical channel (accelerometer) in the basement, the remaining six vertical channels are not deemed essential for most studies that can be envisioned – unless there is need for a specific study (e.g. floor vibrations). Furthermore, for each of the 3rd floor and penthouse recorders, one of the NS-component channels (accelerometers) (e.g. north locations) are not contributing any record that is different than their neighboring location (e.g., south location). Therefore, a total of eight channels potentially could have been used at other locations (e.g. at intersection of grid lines 4 and A, as well as other possible locations). Another useful deployment could have been a triaxial unit as free-field in the immediate vicinity of the building, which would serve as a reference station for ELIF and other buildings on the campus.

[1] Mentioning commercial names does not constitute endorsement by USGS or UAF.

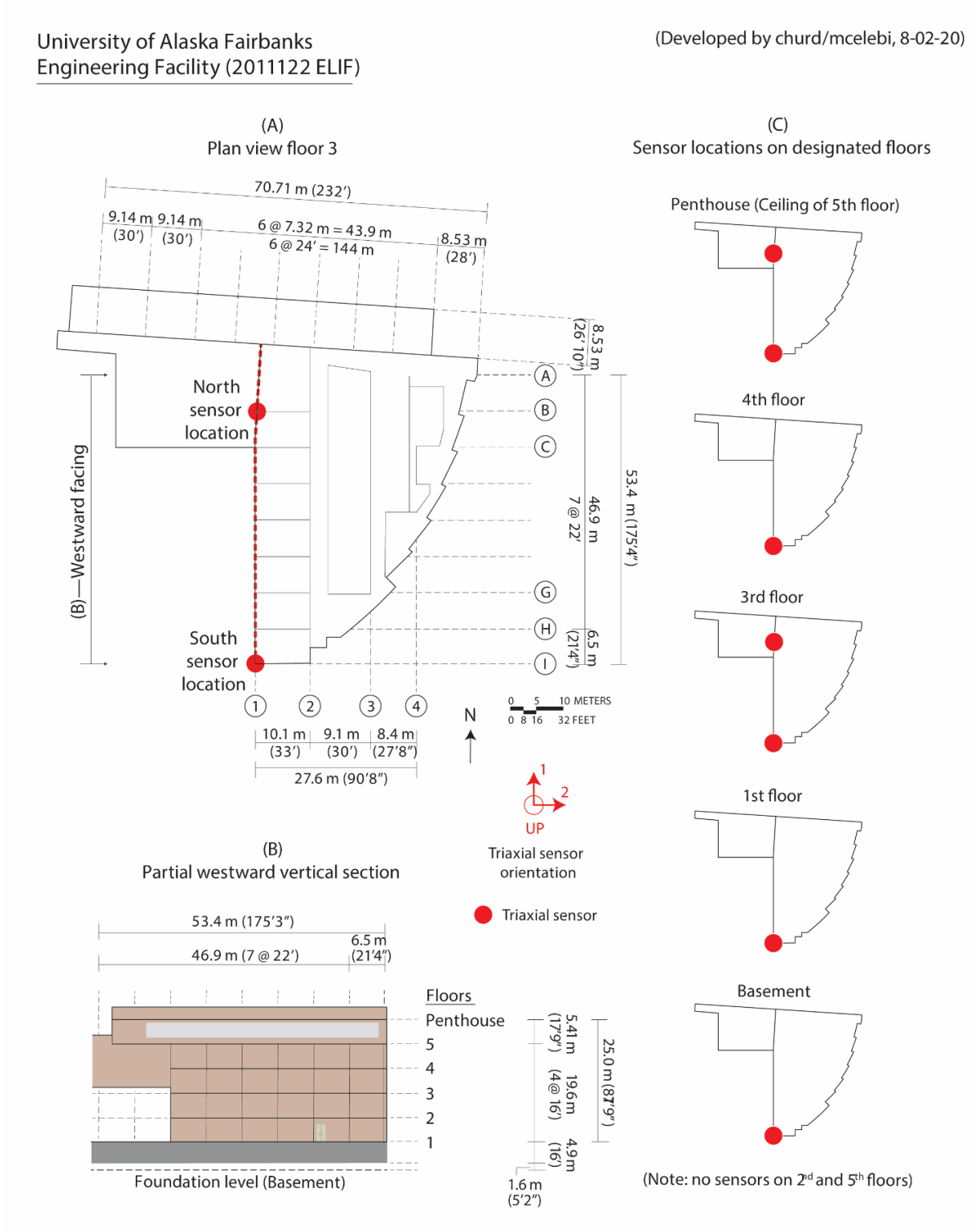

Figure 2. *General schematic plan views, a vertical section of the building, and monitoring array. (A) Plan view of the building (3rd floor) indicates that channels oriented as 1 (NS) are all on grid line 1 and those oriented as 2 (EW) are all in either Grid Line I or B or both as described in (C). (Figure developed using information in structural blueprints of the building).*

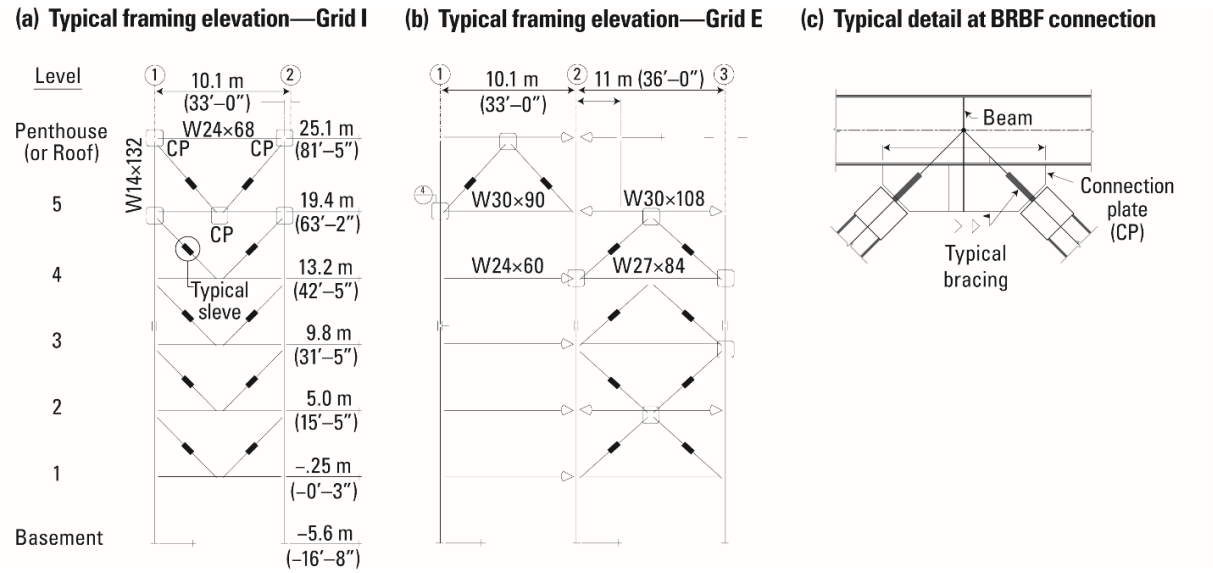

Figure 3. *(a and b) Typical buckling restrained braced framing (BRBF) elevations depicting K-bracing with BRBs and typical details at (c) connections and connection plates (CPs). (Figure developed using information in structural blueprints of the building).*

DATA AND ANALYSIS

Building response motion time series for the analysis have been extracted from a continuous data archive of the Alaska Earthquake Center. Data are recorded at 200 samples per second. Figures 4a-c show the NS, EW, and torsional acceleration time-histories, respectively. Similarly, Figures 4d-f show the NS, EW, and torsional displacement time-histories, respectively. We note that torsional time-histories are obtained only for two floors (3rd and penthouse), where each of the floors have two parallel EW accelerometers. In this paper, torsional acceleration (or displacement) infers the relative difference between two parallel accelerations (or displacements) on the same floor. In other words, we did not divide it by a constant, that is the distance between the two parallel sensors.

Figures 5a-c show NS, EW, and torsional amplitude spectra of accelerations recorded in the north locations (dashed blue lines) and south locations (solid red lines), respectively. Similarly, Figures 5d-e show NS and EW spectral ratios of amplitude spectra at a floor *i* with respect to that at basement, respectively. Note that there is no computed spectral ratio for torsion because there are no torsional data from the basement.

The amplitude spectra and spectral ratios indicate:

a. The frequencies ~1.4 Hz and 1.6 Hz appearing in the amplitude spectra of NS, EW, and torsional accelerations are closely coupled (Figure 5).
b. The frequency ~0.3 Hz appearing in amplitude spectra is the source frequency (Figure 5a-b). It cancels out in the spectral ratios (Figures 5d-e).
c. No plot of spectral ratio for torsional amplitude spectra was possible (so, the blank panel in Figure 5).

Figure 6 shows cross-spectra, phase angles, and coherency plots for accelerations recorded at the south locations (Figure 2) of the penthouse versus those recorded at the 3rd floor for the NS and EW directions. Figures 6a-c show cross-spectrum, phase angle, and coherency, respectively, in the NS direction. Figures 6d-f show cross-spectrum, phase angle, and coherency, respectively, in the EW direction. Torsional accelerations are the differences between EW acceleration in the north and south locations at the penthouse and the 3rd floor. Figures 6g-i show cross-spectrum, phase angle, and coherency, respectively, in the torsional direction. The phase plots show that for all frequencies <3 Hz, motions are in phase with unity coherency – further evidence of coupling and close coupling for the NS and EW motions. For detailed information on cross-spectra, phase angle, and coherency computations, the reader is referred to *Bendat & Piersol* (1980).

Similarly, Figures 7a-f show cross-spectra, phase angles, and coherency plots for accelerations recorded at the south locations (Figure 2) of the penthouse versus those recorded at the basement for the NS and EW directions, respectively. Figures 7g-i show the same plots for the torsional direction for the penthouse and 3rd floor, respectively. For the NS and EW components, whereas there is unity or near-unity coherency, the phase angles do not show that motions are in phase, which can be attributed to travel lag time.

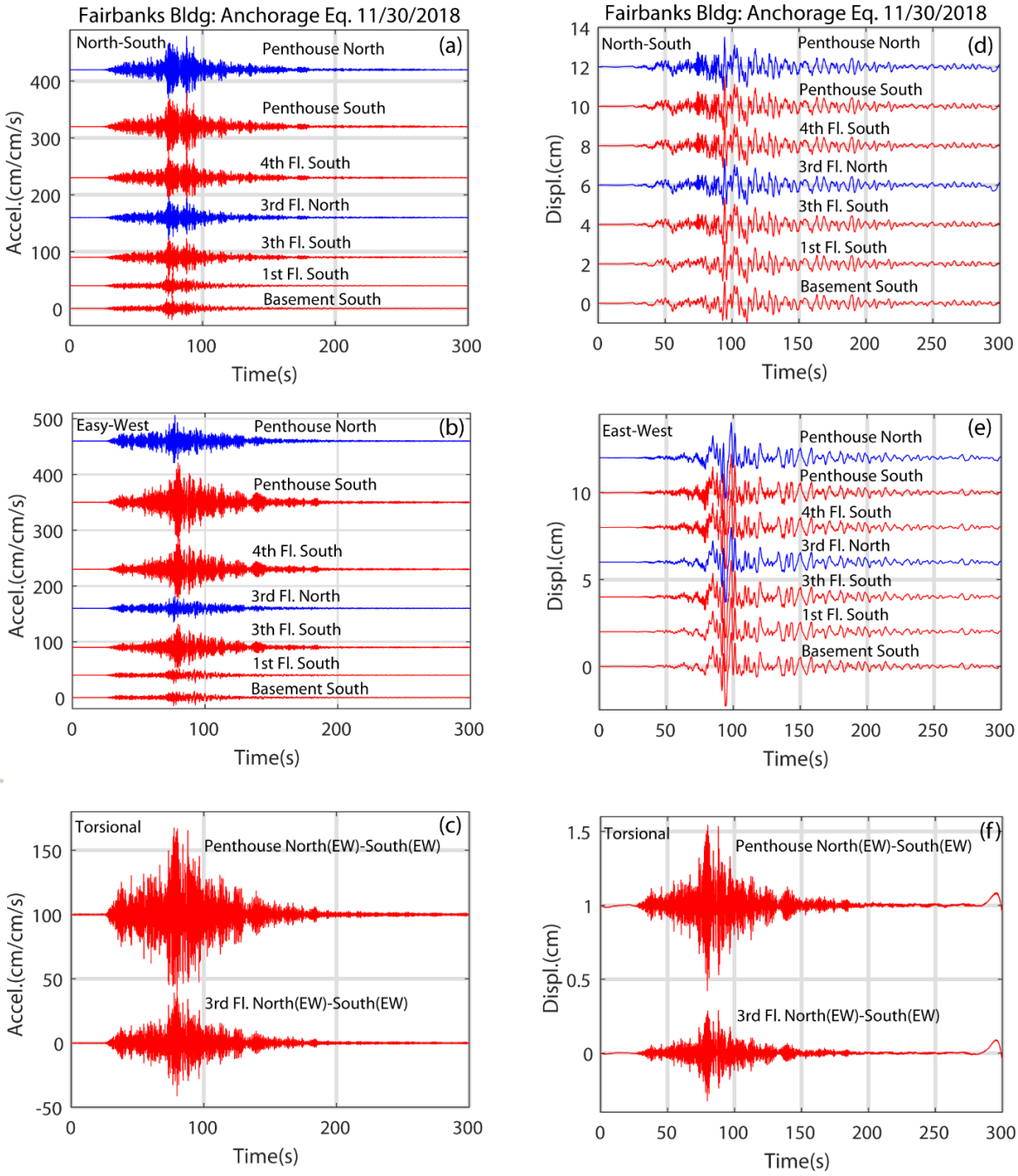

Figure 4. *Panels a, b, and c show NS, EW, and torsional acceleration time-histories, respectively. Panels d, e, and f show NS, EW, and torsional displacement time-histories, respectively. Time histories in red are from channels in the south location and those in blue are from channels in the north location.*

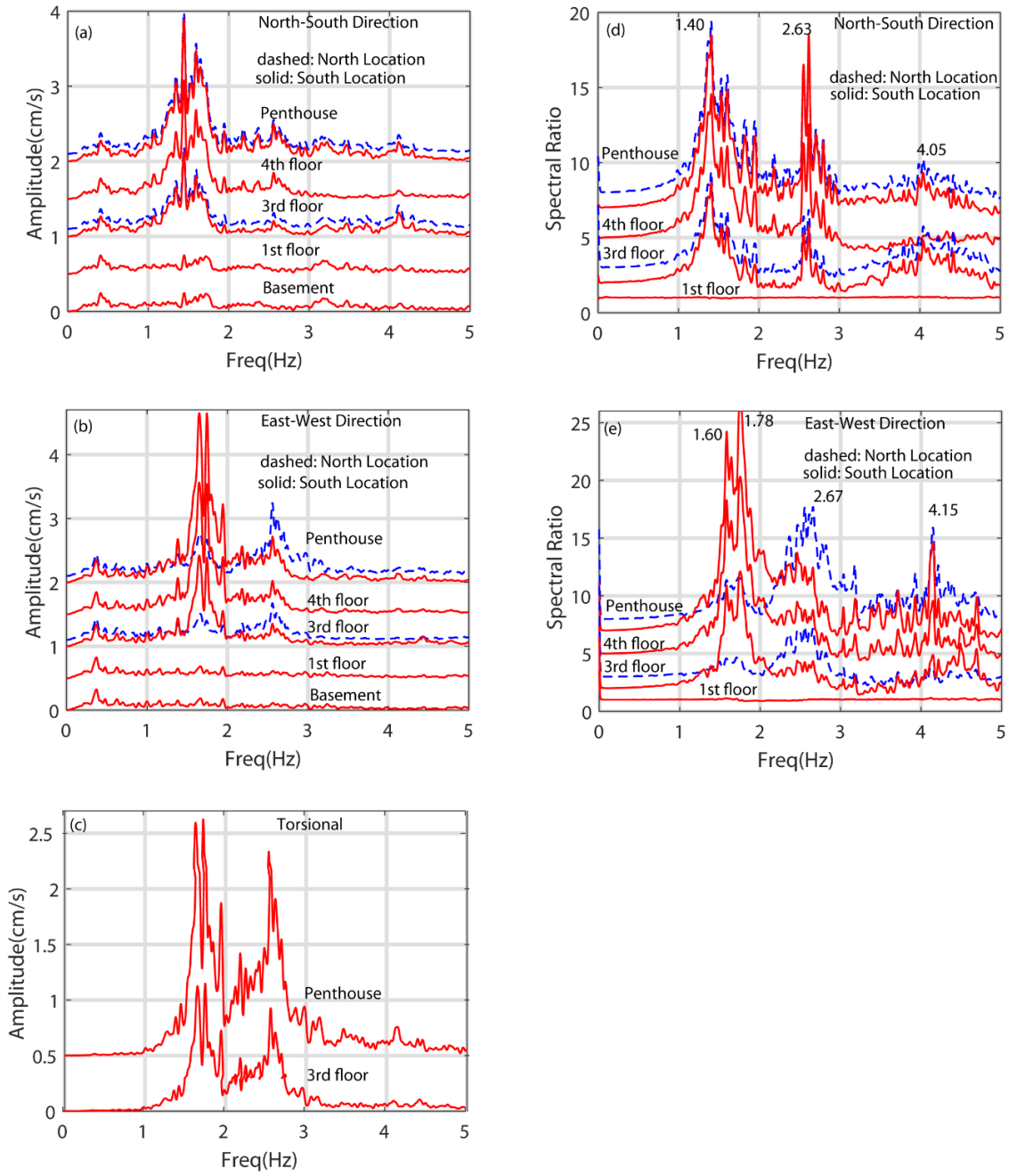

Figure 5. *Panels a, b, and c show NS, EW, and torsional amplitude spectra of accelerations recorded in the north locations (dashed blue lines) and south locations (solid red lines), respectively. Panels d and e show NS and EW spectral ratios of amplitude spectrum at a floor i with respect to that at the basement, respectively. Note that there is no sensor at the north location of the basement; hence, the spectral ratio of the north location (blue-dashed) is with respect to basement south locations. Note also that there is no computed spectral ratio for torsion because there are no torsional data from the basement.*

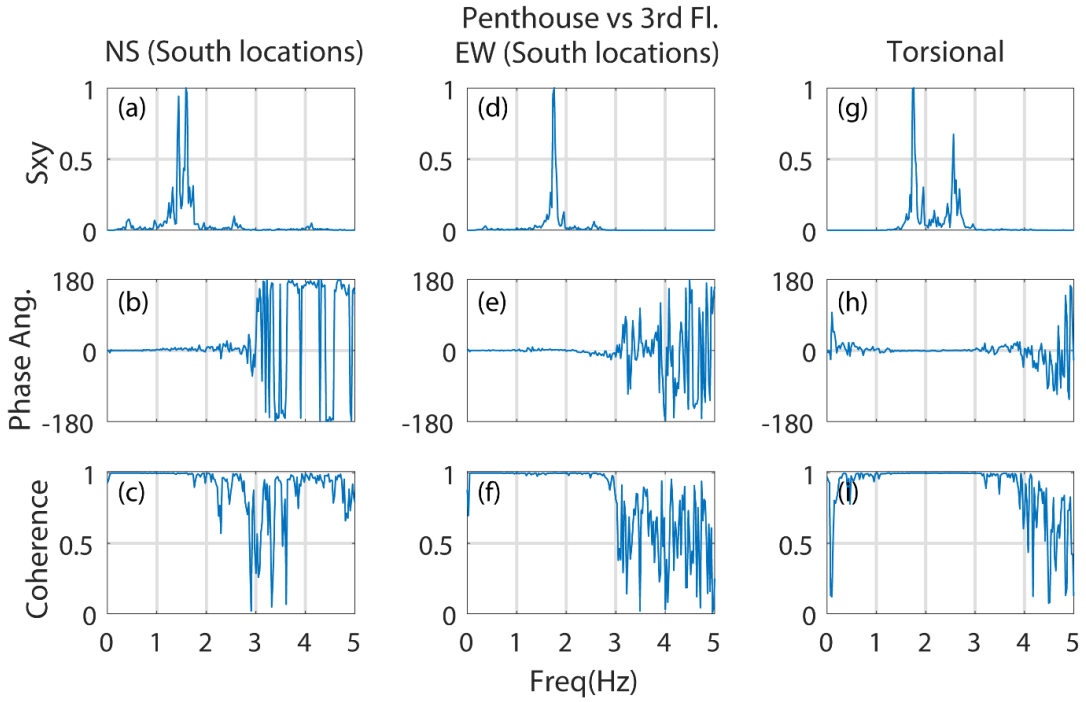

Figure 6. *(a, d, g) Cross-spectra, (b, e, h) phase angles, and (c, f, i) coherency plots for (a, b, c) NS, (d, e, f) EW, and (g, h, i) torsional accelerations recorded at the penthouse and 3rd floor.*

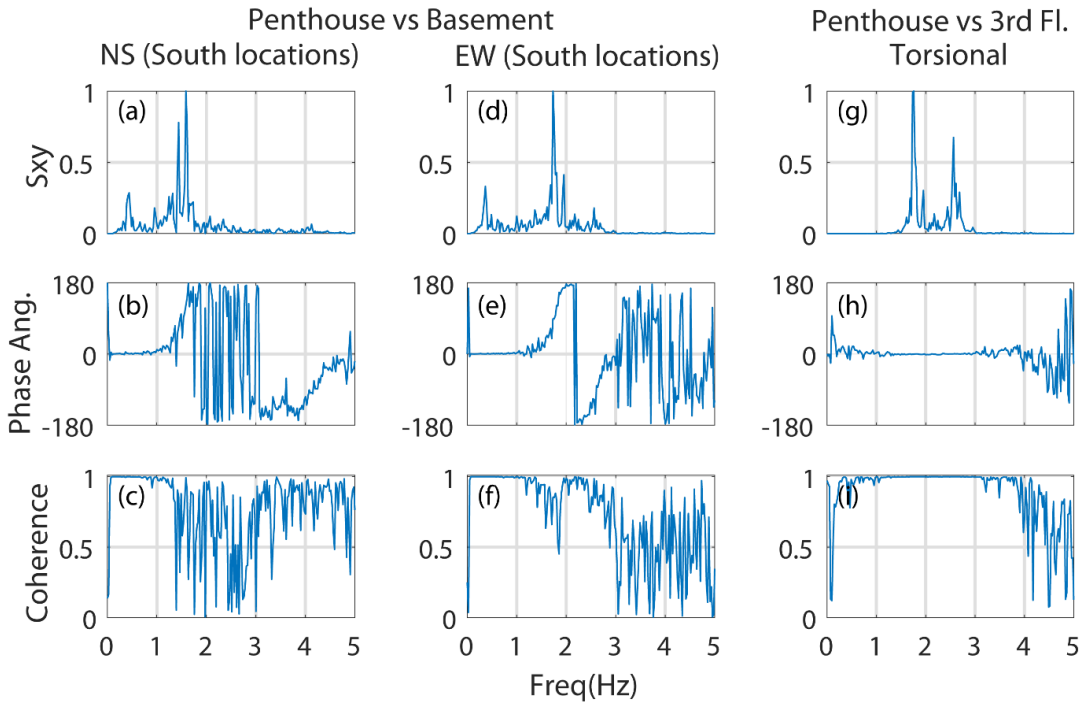

Figure 7. *(a, d, g) Cross-spectra, (b, e, h) phase angles, and (c, f, i) coherency plots for (a, b, c) NS, (d, e, f) EW, and (g, h, i) torsional accelerations (recorded at the penthouse and basement for NS and EW and penthouse and 3rd floor for torsional).*

SYSTEM IDENTIFICATION

System identification utilizes recorded or observed input-output data (e.g. acceleration) to extract mode shapes, structural frequencies, and critical damping percentages. In this paper, the input is the basement (or ground floor) acceleration time-history, and the output is the roof acceleration time-history. The system identification method, ARX (an acronym meaning AR for autoregressive and X for extra input) used in this study is based on the least-squares method for single input-single output. Background information of this method is provided in *Ljung* (1987). The method is readily usable as a coded application in Matlab (Mathworks, 2020 and prior releases).

Figures 8 and 9 show the results of system identification for NS and EW directions, respectively. In each figure, depicted are (a) recorded acceleration time-histories from the basement as input and the penthouse as output and the computed penthouse acceleration time-history, (b) amplitude spectra of recorded and computed output accelerations at the penthouse, and (c) amplitude spectra of recorded input acceleration at the basement. In both figures, the output recorded and computed penthouse accelerations and their amplitude spectra in frames (b) are comparable. As a result, for the NS direction, a frequency of f = 1.47 Hz, and a critical damping percentage of ξ = 7.2 are identified. Similarly, for the EW direction, f = 1.69 Hz, and ξ = 4.7 are identified. We can deduce that the identified frequencies are similar to those determined from spectral methods. The critical damping percentages, on the other hand, are considered to be high for such low-amplitude shaking of the building. Unfortunately, the instrumentation design does not allow us to pinpoint how much the damping capacity is enhanced by the BRBF at this low-level shaking.

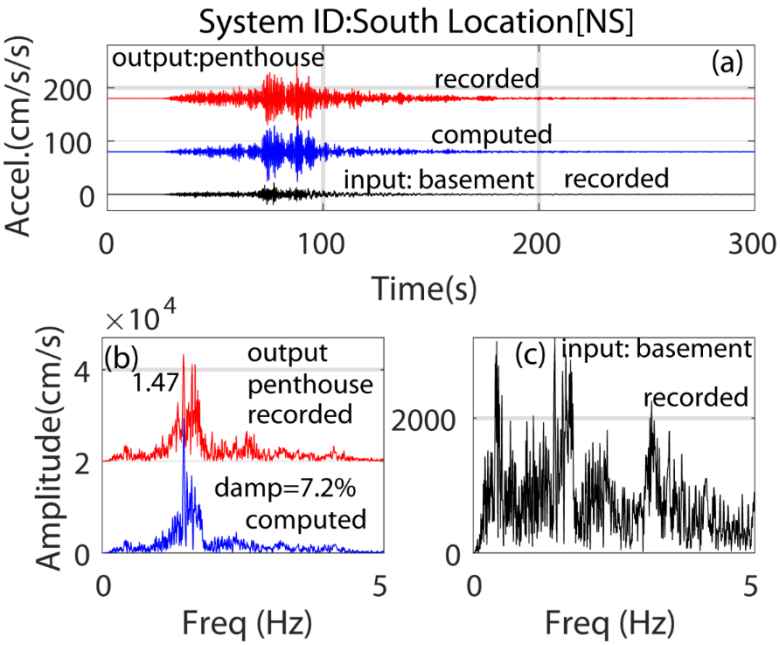

Figure 8. *System identification of NS accelerations at south locations.*
(a) NS channels at the south basement location and penthouse are used as input and output, respectively. The plot also shows the computed penthouse acceleration using the ARX method.
(b) Amplitude spectra of recorded and computed accelerations at the penthouse.
(c) Amplitude spectrum of acceleration at the basement used as input.

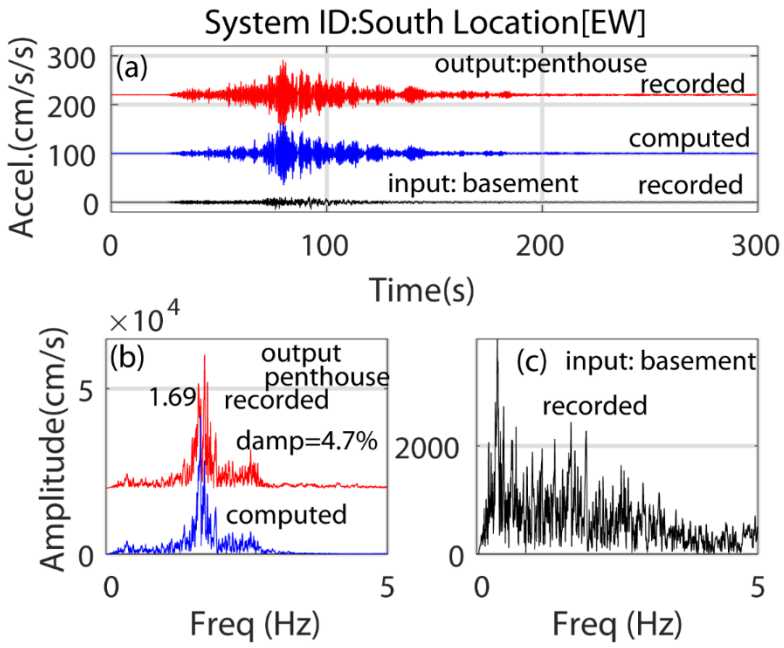

Figure 9. *System identification of EW accelerations at south locations.*
(a) EW channels at the south basement location and penthouse are used as input and output, respectively. The plot also shows the computed penthouse acceleration using the ARX method.
(b) Amplitude spectra of recorded and computed accelerations at the penthouse.
(c) Amplitude spectrum of acceleration at the basement used as input.

DISCUSSION

With low-amplitude shaking recorded at an epicentral distance of ~400 km from the M7.1 earthquake, the displacements of the building are not expected to be large (Figures 4d-e). In addition, because this building has several bays with K-configured BRBFs, the displacements are expected to be smaller than if the building did not have the braces. Table 2 shows a summary of the displacements computed from the accelerations in both NS and EW directions and at each of the north and south locations of sensors. From these, we computed the largest relative displacements between the penthouse and 1st floor. We used the 1st floor because the displacements at the 1st floor and basement are very similar, and this allows us to have a larger average drift ratio, due to smaller denominator. The largest average drift ratio is ~ 0.028% (Table 2), which is smaller than a drift ratio that indicates the onset of damage (e.g. 0.5%) [*Kubo et al*., 2011; The Building Standards Law of Japan [BCJ 2001a and 2001b]; *Çelebi et al*., 2016].

Table 2. *Summary of peak displacements, peak relative displacements and average drift ratios in the NS and EW directions.*

South Locations						North Locations	
Peak Displacements (cm)							
at	Penthouse	4th	3rd	1st	Basement	Penthouse	3rd
NS	1.52	1.45	1.35	1.15	1.10	1.51	1.35
EW	2.42	2.38	2.35	2.28	2.28	1.52	1.35
Peak Relative Displacements (cm)							
	Between 5th and 1st fl					Between 5th and 3rd fl	
NS	0.69					0.13	
EW	0.65					0.31	
Ave. Drift Ratio (%)							
	Divide by 25.0 m (height between 5th and 1st fl)					Divide by 15.21 m	
NS	0.028					.0089	
EW	0.026					.02	

Table 3. *Summary of frequencies (periods) and critical damping percentages identified for the first mode using spectral ratios and system identification.*

	Freq(Hz)/ Period[s] (f/T)			Damping (%) (ξ)	
Mode	NS	EW	Torsional	NS	EW
	Spectral Ratios				
1	1.40/0.73	1.60/0.63	1.78/0.56		
	System Identification				
1	1.47/0.68	1.69/0.59		7.2	4.7

CONCLUSIONS

A seismic structural recording array installed in 2017 at the Engineering Learning and Innovation Facility building on the University of Alaska, Fairbanks campus recorded a distant M7.1 earthquake in Anchorage, Alaska, on November 30, 2018. Recorded structural response data allow limited system identification analyses, including the calculation of spectral ratios. As a result, only the first modal dynamic response characteristics were identified (Table 3). The NS, EW, and torsional modes are coupled (Figure 5). At low-shaking levels, the identified critical damping percentages are significantly high - at usual design levels. It is not clear if the BRBFs contributed to the critical damping percentages. With a limited number of sensors, it is difficult to quantify the contribution of BRBFs. In the future, at least in one area of BRBFs, deployment of a dynamic displacement transducer to measure and assess the BRBFs contribution to damping by those structural elements could be done. As expected, at a low level of shaking, average drift ratios are small (Table 2) and at approximately 5% of the drift ratio level of the start of inelastic behavior.

Acknowledgements
This research was supported in part by the Geophysical Institute, University of Alaska Fairbanks. The views and conclusions contained in this document are those of the authors and should not be interpreted as representing the opinions or policies of the U.S. Geological Survey. Any use of trade, firm, or product names is for descriptive purposes only and does not imply endorsement by the U.S. Government.

Data and Resources:
Waveform data provided by the Alaska Earthquake Center, University Alaska Fairbanks (earthquake.alaska.edu). MATLAB based tools were used for data analysis.

References

Bendat, J. S., and Piersol, A. G. (1980). *Engineering Applications of Correlation and Spectral Analyses*, John Wiley & Sons, New York, NY, 302 pp.

Çelebi, M. (2019). Highlights of a cursory study of behavior of three instrumented buildings during the Mw 7.1 Anchorage, Alaska, Earthquake of 30 November 2018, *Seism. Res. Lett. 91*, doi: 10.1785/0220190220.

Çelebi, M., Ulusoy, H., and Nakata, N. (2016). Responses of a tall building in Los Angeles, California as inferred from local and distant earthquakes, *Earthquake Spectra 32(3)*: 1821–1843.

IBC (International Building Code) 2009 edition, International Code Council, Inc. 4051 West Flossmoor Road, Country Club Hills, IL 60478.

Kubo, T., Hisada, Y., Murakami, M., Kosuge, F., and Hamano, K. (2011). Application of an earthquake early warning system and a real-time strong motion monitoring system in emergency response in a high-rise building, *Soil Dynamics and Earthquake Engineering 31*, 231–239.

Ljung, L. (1987). System Identification: Theory for the User, Prentice Hall, Englewood Cliffs, NJ.

Mathworks, 2020 and previous versions. Matlab and Toolboxes, South Natick, MA.

Pewe, T.L., Bell, J.W., Forbes, R.B., and Weber, F.R. (1976). Geologic map of the Fairbanks D-2 SW quadrangle, Alaska, https://ngmdb.usgs.gov/Prodesc/proddesc_9655.htm.

The Building Center of Japan (BCJ) (2001a). Time history response analysis building performance evaluation manual, Technical Appraisal Department, Structural Safety Section Report No: BR KO-02-01 (adopted 1 June 2000, amended 25 April 2001).

The Building Center of Japan (BCJ) (2001b). Manual for time history response analysis of building performance evaluation manual, Technical Appraisal Department, Structural Safety Section Report No: BR KO-02-01 (adopted 1 June 2000, amended 25 April 2001).

West, M. E., A. Bender, M. Gardine, L. Gardine, K. Gately, P. Haeussler, W. Hassan, F. Meyer, C. Richards, N. Ruppert, C. Tape, J. Thornley, and R. Witter (2019). The 30 November 2018 Mw 7.1 Anchorage earthquake, *Seismological Research Letters*, doi: 10.1785/0220190176.

Wilson, F.H., Hults, C.P., Mull, C.G, and Karl, S.M. (2015). Geologic map of Alaska, https://ngmdb.usgs.gov/Prodesc/proddesc_103832.htm.